Science of Remote Sensing 10 (2024) 100162

Contents lists available at ScienceDirect

Science of Remote Sensing

journal homepage: www.sciencedirect.com/journal/science-of-remote-sensing

Enhancing the temporal resolution of water levels from altimetry using D-InSAR: A case study of 10 Swedish Lakes

Saeid Aminjafari [a,*], Frédéric Frappart [b], Fabrice Papa [c,d], Ian Brown [a], Fernando Jaramillo [a,e]

[a] Department of Physical Geography and Bolin Centre for Climate Research, Stockholm University, SE–106 91, Stockholm, Sweden
[b] INRAE, UMR1391 ISPA, 33140, Villenave d'Ornon, France
[c] LEGOS, Université de Toulouse (CNES/CNRS/IRD/UPS), 14 Avenue Edouard Belin, 31400, Toulouse, France
[d] Universidade de Brasília, Institute of Geosciences, Campus Universitario Darcy Ribeiro, 70910-900, Brasilia, DF, Brazil
[e] Baltic Sea Centre and Stockholm Resilience Center, Stockholm University, SE-106 91, Stockholm, Sweden

ARTICLE INFO

Keywords:
D-InSAR
Lake water levels
Satellite altimetry
DInSAlt

ABSTRACT

Lakes provide societies and natural ecosystems with valuable services such as freshwater supply and flood control. Water level changes in lakes reflect their natural responses to climatic and anthropogenic stressors; however, their monitoring is costly due to installation and maintenance requirements. With its advanced hardware and computational capabilities, altimetry has become a popular alternative to conventional in-situ gauging, although subject to the temporal availability of altimetric observations. To further improve the temporal resolution of altimetric measurements, we here combine radar altimetry data with Differential Interferometric Synthetic Aperture Radar (D-InSAR), using ten lakes in Sweden as a testing platform. First, we use Sentinel-1A and Sentinel-1B SAR images to generate consecutive six-day baseline interferograms across 2019. Then, we accumulate the phase change of coherent pixels to construct the time series of InSAR-derived water level anomalies. Finally, we retrieve altimetric observations from Sentinel-3, estimate their mean and standard deviation, and apply them to the D-InSAR standardized anomalies. In this way, we build a water-level time series with more temporal observations. In general, we find a strong agreement between water level estimates from the combination of D-InSAR and Satellite Altimetry (DInSAlt) and in-situ observations in eight lakes (Concordance Correlation Coefficient - CCC >0.8) and moderate agreement in two lakes (CCC >0.57). The applicability of DInSAlt is limited to lakes with suitable conditions for double-bounce scattering, such as the presence of trees or marshes. The accuracy of the water level estimates depends on the quality of the altimetry observations and the lake's width. These findings are important considering the recently launched Surface Water and Ocean Topography (SWOT) satellite, whose capabilities could expand our methodology's geographical applicability and reduce its reliance on ground measurements.

1. Introduction

Lakes are freshwater stocks supporting significant aquatic biodiversity and lacustrine ecosystems (Barzegar et al., 2021). They also play a key role in the hydrological cycle and act as indicators of climate change due to their high sensitivity to changing hydro-climatic conditions (Kao et al., 2020; Magsar et al., 2021; Woolway et al., 2020; Zhang et al., 2020). The nature- and human-driven changes in seasonal and inter-annual water levels regulate water quality and quantity in these water bodies (Myrzakhmetov et al., 2022; Yao et al., 2021). Prior to extreme changes in a lake's status, water levels can show early warning signs and supply information for sustainable water management (Barzegar et al., 2021), mitigating risks related to the ecosystem service of freshwater provision (Myrzakhmetov et al., 2022).

To understand how water availability is changing in the world's lakes and to be able to attribute these changes to specific climatic and human drivers, we must first track changes in the amount of freshwater in the lakes (Cooley et al., 2021). This includes changes in water extent, level, and corresponding variations in stored water volume. Lake water levels can be measured on-site with gauges. However, this is done only in a few locations worldwide, and the number of gauging stations is declining due to the costly maintenance and installation in remote lakes (Alsdorf et al., 2007; Aminjafari et al., 2024a; Cooley et al., 2021; Shiklomanov et al., 2002). Lake water levels can also be tracked using

* Corresponding author.
E-mail address: saeed.aminjafari@natgeo.su.se (S. Aminjafari).

https://doi.org/10.1016/j.srs.2024.100162
Received 18 June 2024; Received in revised form 16 August 2024; Accepted 6 September 2024
Available online 10 September 2024

airborne technologies such as Lidar/Radar and photogrammetry (Bandini et al., 2017; Ridolfi and Manciola, 2018), which, although accurate, can only provide a snapshot in time of water levels and expensive flight operations do not permit high temporal resolutions.

Radar altimetry missions were initially launched to determine the marine geoid and sea level and are now used for measuring the water levels of lakes and rivers along their track (Abdalla et al., 2021; Cretaux et al., 2017). Satellite altimeters transmit Laser or Radar signals in a Nadir-looking direction and measure the water level based on the signal's travel time. With the advances in new technology and processing techniques, satellite altimeter sensors can now measure water levels over the ocean and freshwater bodies (Abdalla et al., 2021; Bandini et al., 2017; Markus et al., 2017; Zhang et al., 2011). For instance, smaller footprints and higher along-track resolutions of lake water levels can be obtained with the Synthetic Aperture Radar (SAR) mode of altimetric sensors (e.g., Sentinel-3, Sentinel-6, and Cryosat-2; Abileah and Vignudelli, 2021) and using higher frequency signals (Ka instead of Ku band) on Satellite with ARgos and ALtiKa (SARAL) altimeter sensor (Verron et al., 2021). Recent developments in Fully Focused Synthetic Aperture Radar (FFSAR) technology have shown that off-nadir water levels can also be derived, significantly enhancing spatial coverage and resolution (Boy et al., 2023). This advancement could mitigate some spatial limitations previously attributed to nadir altimetry. Furthermore, the quality of altimetry observations has also increased with the uploading of the elevation data on the sensors by Open-Loop Tracking Command (instead of the older Closed Loop), which increases the positioning of the receiving window, especially for water bodies in mountainous areas (Biancamaria et al., 2017, 2018; Taburet et al., 2020).

As the presence of a bright target in the altimeter's footprint is essential for measuring water level, single-sensor altimetry over small lakes (along-track width $\leq$200 m) sometimes results in low coverage (Baup et al., 2014) and low temporal resolutions (e.g., 27 days for Sentinel-3, and 91 days for ICESat-2). With multi-sensor altimetry, a higher number of satellite ground tracks pass over the water surface, leading to improved temporal resolution (Biancamaria et al., 2017). To further enhance the temporal resolution of satellite altimetry, it is necessary to combine altimetry data with other technologies.

Synthetic Aperture Radar (SAR) retrieves the phase and amplitude of the received signal. Differential Interferometric SAR (D-InSAR) is the process of calculating SAR phase differences between two SAR images of a specific location at two different times, delivering information on water level changes (Alsdorf et al., 2000; Aminjafari et al., 2024b; Jaramillo et al., 2018; Liu et al., 2020; Palomino-Ángel et al., 2022). Many studies have used D-InSAR with long- (L-band) and short- (C-band) wavelength SAR sensors to retrieve water-level relative changes between neighboring pixels over water surfaces covered by vegetation. These characteristics provide the necessary coherence of the SAR signal for phase unwrapping (Chen et al., 2020; Hong et al., 2010; Siles et al., 2020; Wdowinski et al., 2008).

In the case of open water bodies (e.g., lakes), the SAR signal is mainly incoherent and spatially discontinuous, limiting phase unwrapping (Alsdorf et al., 2000). However, recent studies have found that the accumulated phase changes of the high-coherence individual pixels on the lake surface do correlate with hydrological observations (Aminjafari et al., 2024b; Palomino-Ángel et al., 2022). Based on this finding, we propose a new method using D-InSAR to support satellite altimetry by improving its temporal resolution.

2. Methods and materials

2.1. Study area

Amongst more than 100,000 lakes in Sweden (Larson, 2012), less than 1% have long and continuous gauged water level observations (Aminjafari et al., 2024a, 2024b). This low number highlights the challenges of their monitoring. These daily lake water level observations, some dating back to the 1930s, are recorded by the Swedish Meteorological and Hydrological Institute (SMHI). Among lakes with in-situ data, ten fall under the ground tracks of the Sentinel-3A/B satellites (Fig. 1 and Table 1). We use D-InSAR and satellite altimetry data in these lakes to construct a water level time series with at least six-day intervals, which we validate with gauge observations.

2.2. Methods

In summary, we generate six-day interferograms between Sentinel-1A/B SAR pairs in ice-free months in 2019 in ten lakes in Sweden. After identifying high-coherence pixels on the lake surface area in all interferograms, we accumulate their InSAR-derived phase change from the first to the last interferogram. If the accumulated phase change correlates with actual water level observations, we assume their normalized anomalies are identical. Hence, we apply the standard deviation and the average of the altimetry-based water levels to the water level anomalies derived from D-InSAR to obtain a high temporal resolution (less than six days) time series of water levels.

2.3. D-InSAR theory and data

In this study, we build on the methodology introduced by Aminjafari et al. (2024b), which assesses the application of D-InSAR for water level change calculations in lakes, to estimate lake water level anomalies (i.e., deviation from the average). While in the middle of a lake, the transmitted signal from the Radar sensor bounces in a different direction than in the satellite Line Of Sight (LOS), resulting in zero temporal coherence of the SAR signal; in the vicinity of a lake, the vegetation cover can reflect the signal from the water surface to the satellite, resulting in high coherence (Aminjafari et al., 2024b). The so-called double bounce mechanism can happen in sporadic pixels near the lake's shoreline, where trees and marshes are common.

First, we calculate the phase difference between pairs of SAR images with six-day temporal baselines to estimate water level changes. The phase difference ($\Delta\varphi$) for each pixel is extracted from the interferogram and has four main components: the ground target's displacement ($\Delta\varphi_d$), the stereoscopic effect of the Earth's topography ($\Delta\varphi_{topo}$), the difference between the two acquisitions' geometry ($\Delta\varphi_{geo}$), and atmospheric phase delays and instrument's noise ($\Delta\varphi_{other}$) (Aminjafari et al., 2024b):

$$\Delta\varphi = \Delta\varphi_d + \Delta\varphi_{topo} + \Delta\varphi_{geo} + \Delta\varphi_{other} \quad (1)$$

We remove $\Delta\varphi_{topo}$, $\Delta\varphi_{geo}$, and $\Delta\varphi_{other}$ with a Digital Elevation Model (DEM), orbital information of the satellite at the acquisition times, and spectral and band filtering to obtain $\Delta\varphi$ as $\Delta\varphi_d$. After finding the equivalent pixels in the two images, the cross-correlations between them (called coherence; C) and the phase change are generated and filtered by the adaptive Goldstein filter (Goldstein and Werner, 1998). The interferometric quality of pixels is shown by coherence values (0–1; full noise to no noise). To ensure the consistency of high-coherence pixels over time, we assess the coherence of these pixels across all interferograms throughout the study period. While coherence can vary slightly due to environmental changes, we choose pixels that consistently exhibit coherence values larger than 0.25 (Aminjafari et al., 2024b).

We apply the tropospheric correction to interferogram phase change by using the atmospheric datasets provided by the Generic Atmospheric Correction Online Service for InSAR (GACOS) (Yu et al., 2017, 2018a, 2018b) based on the High-Resolution ECMWF weather model (The European Center for Medium-Range Weather Forecasts), Shuttle Radar Topography Mission (SRTM) DEM (Farr and Kobrick, 2000), and Advanced Spaceborne Thermal Emission and Reflection Radiometer (ASTER) GDEM (Abrams et al., 2020). We calculate the equivalent atmospheric phase change between the six-day consecutive Sentinel-1 images and subtract the troposphere-corrected phase change of a

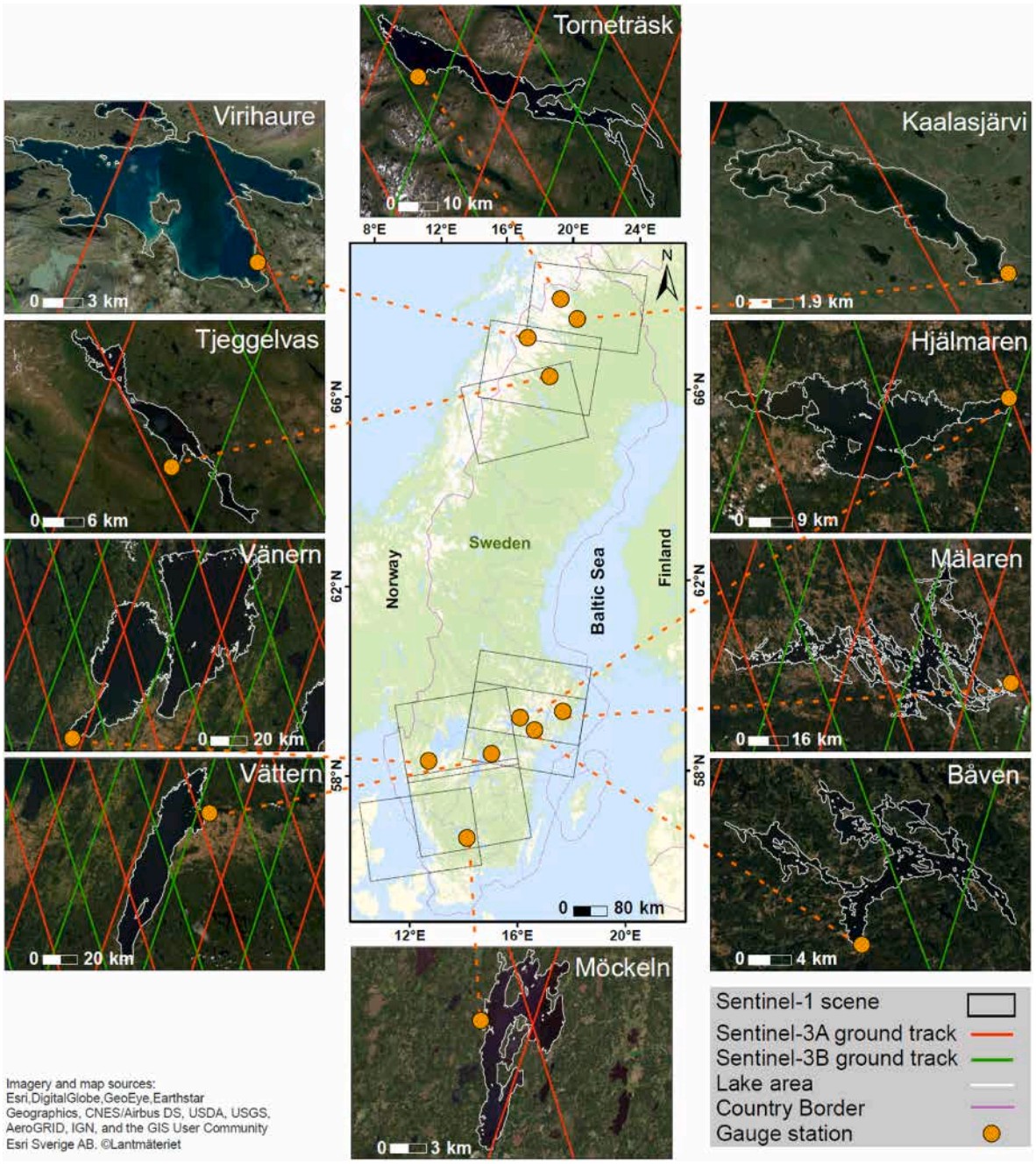

Fig. 1. The ten lakes in Sweden with in-situ water levels, altimetry tracks of the Sentinel-3A/B sensor (lake panels) and Sentinel-1 SAR scenes over the lakes (center panel).

geodetic reference point from the troposphere-corrected phase change of pixels on the water surface. To further minimize the tropospheric phase delay, we choose the reference points within one km distance from the lakes' shores and calculate the uncertainty of the D-InSAR estimations inside a 1×1 km^2 area containing the reference point (Aminjafari et al., 2024b).

When six-day in-situ water level changes seldom exceed a full cycle of SAR signal, the time series of consecutive interferograms for each pixel has been found to correlate with the time series of in-situ water levels (Aminjafari et al., 2024b). The vertical component of the phase change for each pixel (Δh_D) is calculated by the sensor's wavelength ($\lambda = 5.6$ cm for Sentinel-1) and incidence angle (θ), which represents the direction of the changes in water level (Aminjafari et al., 2024b):

$$\Delta h_D = \frac{\lambda * \Delta\varphi_p}{4\pi * cos\ \ cos\,\theta} \tag{2}$$

By accumulating Δh_D from the first interferogram to the last one, we can obtain water levels (h_D) relative to the water level of the first acquisition (Aminjafari et al., 2024b) as:

$$h_D = \sum_{i=1}^{i=n} \Delta h_D^i \tag{3}$$

where n is the total number of interferograms. To have a similar vertical reference for validation purposes, we set the water level height at the first acquisition date to zero for both D-InSAR- and gauged water levels (h_D and $h_{G,}$ respectively).

Table 1
The physical characteristics of 10 lakes in Sweden with three sources of water level data: in-situ, satellite altimetry, and D-InSAR.

Lake name	Gauge name	Area (km^2)	Max depth (m)	Mean depth (m)	Length/ Width	Elevation (m asl)
Torneträsk	Abisko	332	168	51.8	6.36	341
Kaalasjärvi	Kaalasjärvi	16.4	0	0	4.94	461
Virihaure	Staloluokta	112	130	39.4	1.80	579
Tjeggelvas	Stenudden	66.9	65	–	6.67	450
Mälaren	Mälaren	1072	64	13	1.85	0.7
Hjälmaren	Hjälmaren	483	20	6.2	3.00	22
Båven	Sibro2	64	48	9.4	9.20	21.1
Vättern	Motala	1893	128	39.5	4.35	88.5
Vänern	Vänern W	5650	106	27	1.85	44
Möckeln	Möckeln	46	10	2.8	2.73	136

Table 2
Sentinel-1 data for each lake. Column "A/D" shows the sensor transition pass (Ascending/Descending).

Lake	# of images	Interval in 2019	Path	Frame	A/D
Torneträsk	25	19 May-10 Oct	95	365	D
Kaalasjärvi	25	19 May-10 Oct	95	365	D
Virihaure	28	20 May-29 Oct	29	218	A
Tjeggelvas	25	24 May-15 Oct	168	369–370	D
Mälaren	29	19 May-3 Nov	95	395	D
Hjälmaren	29	19 May-3 Nov	95	395	D
Båven	29	19 May-3 Nov	95	395	D
Vättern	29	24 May-8 Nov	175	187	A
Vänern	42	19 Mar-25 Nov	73	190	A
Möckeln	43	17 Mar-30 Nov	146	183	A

We obtained 221 Sentinel-1A/B images from the National Aeronautics and Space Administration's (NASA) Alaska Satellite Facility Distributed Active Archive Center (ASF DAAC) to generate 214 interferograms with a six-day temporal resolution (Table 2). The images cover late spring to late autumn in 2019, when the lakes' surface areas are not frozen (Fig. 1 and Table 2). For the lakes above 60° latitude, we use the ASTER DEM 30-m resolution, and for the lakes below 60° latitude, SRTM DEM 30-m resolution for co-registration to remove the topographic phase and be able to geocode the interferograms and coherence maps.

2.4. Satellite altimetry theory and data

Radar altimeters measure the distance in the nadir direction between the satellite and the surface of the Earth (or range; R) by emitting a microwave signal (23.8 and 36.5 GHz for Sentinel-3). Altimeter-based geodetic heights are obtained by removing the range and several corrections accounted for delays caused by the path through the atmosphere and geophysical corrections from the orbit height (H_s). To obtain the orthometric height (h_A), it is necessary to subtract the geoid height (Frappart et al., 2021):

$$h_A = H_S - \left(R + C_{ion} + C_{dry} + C_{wet} + C_{solid\ Earth} + C_{pole}\right) - N \quad (4)$$

where C_{ion}, C_{dry}, and C_{wet} are the corrections for the atmospheric delay related to the ionosphere and dry and wet components of the troposphere, calculated with atmospheric models (Frappart et al., 2021), and $C_{solid\ Earth}$ and C_{pole} are the corrections for the Earth's crustal movements caused by the solid-Earth and pole tides, N is the geoid height given by EGM2008. Range values are obtained from the Ice-1 retracker based on the Offset Center of Gravity (OCOG) retracking algorithm (Bamber, 1994; Wingham et al., 1986) which is commonly used for retrieving water levels of inland water bodies (e.g., Frappart et al., 2006).

The Sentinel-3A and Sentinel-3B satellite altimetry data (GDR; Geophysical Data Records) were provided by the Center for Topographic Studies of the Ocean and Hydrosphere (CTOH). The European Space Agency (ESA) launched the two satellites in 2016 and 2018 on the same orbit with a 180° phase shift and a 27-day revisit time. The ground tracks crossing each lake are shown and listed in Fig. 1 and Table 3. We use the Altimetry Time Series software (AlTiS), developed by CTOH (Frappart et al., 2021), to clean the data from outliers and land-contaminated signals before deriving altimetry-based water levels. The AlTiS is a Python-based software with a Graphical User Interface that allows users to manually exclude invalid data by displaying different variables in GDR files such as R, atmospheric and tide corrections, and retracked water level heights. To obtain the time series of water levels from Sentinel-3A/B GDR files, we crop the data outside surrounding the lakes in the AlTiS software and manually remove the outliers. The data cleaning is a gradual process; first, the outliers are vividly distinguishable from the valid data, but, after several steps of data cleaning, the remaining outliers are difficult to locate, and the standard deviation of water levels varies in a low range compared to the range of the data itself. For example, we show the software outputs for Lake Möckeln in Figs. S1 and S2. We select only the ground tracks with fewer outliers

Table 3
Sentinel-3 data for each lake and the maximum lake coverage of ground tracks.

Lake	Pass number (all available tracks)	Pass number (tracks used)	Max lake coverage (km)	Cycle period
Torneträsk	S3A-16, 197, 130 S3B-311, 244, 130	S3A-16, 197, 130 S3B-311, 244, 130	11	17-Mar-2016 9-Dec-2021
Kaalasjärvi	S3A-197, 244	S3A-197	1.9	12-May-2016 2-Nov-2021
Virihaure	S3A-672, 511	S3A-672, 511	6.1	9-Mar-2016 8-Dec-2021
Tjeggelvas	S3A-511, 130 S3B-244	S3A-511, 130	4.5	13-Apr-2016 8-Dec-2021
Mälaren	S3A-369, 44, 483, 158, 597 S3B-44, 483, 158, 597, 272	S3B-44, 483, 158	17.5	6-Dec-2018 6-Dec-2021
Hjälmaren	S3A-255, 700, 369 S3B-44, 369, 700	S3A-255, 700, 369 S3B-44, 369, 700	14.5	10-Mar-2016 3-Dec-2021
Båven	S3B-483, 158	S3B-483, 158	2.7	6-Dec-2018 6-Dec-2021
Vättern	S3A-141, 27 S3B-141, 700	S3A-141, 27 S3B-141, 700	23.6	13-Apr-2016 5-Dec-2021
Vänern	S3A-358, 683, 27, 472 S3B- 683, 472, 27, 141	S3A-358, 683, 27, 472	65	3-Jan-2014 1-Apr-2022
Möckeln	S3A-683, 700	S3A-683, 700	6.6	9-Mar-2016 18-Nov-2021

based on trial and error for each lake. So, a low standard deviation is achieved faster in data cleaning with the selected tracks than all available tracks (Table 3). During the manual data cleaning in AlTiS, we aim at a maximum standard deviation of 25 cm for each epoch of altimetry observations, as shown in Fig. S2. Then, we take the median of all observations within that epoch.

2.5. DInSAlt: combining D-InSAR and satellite altimetry to estimate high-temporal resolution lake water levels

The schematic process of DInSAlt is illustrated in Fig. 2. Aminjafari et al. (2024b) showed that in a pixel on the lake surface and close to the forest and marsh-dominated land covers, the D-InSAR water levels (h_D) and the gauged water levels (h_G) have high Pearson's correlation coefficient (R) and low Lin's concordance correlation coefficient (CCC). Since the direction of the change in h_D and h_G generally agree (high R),

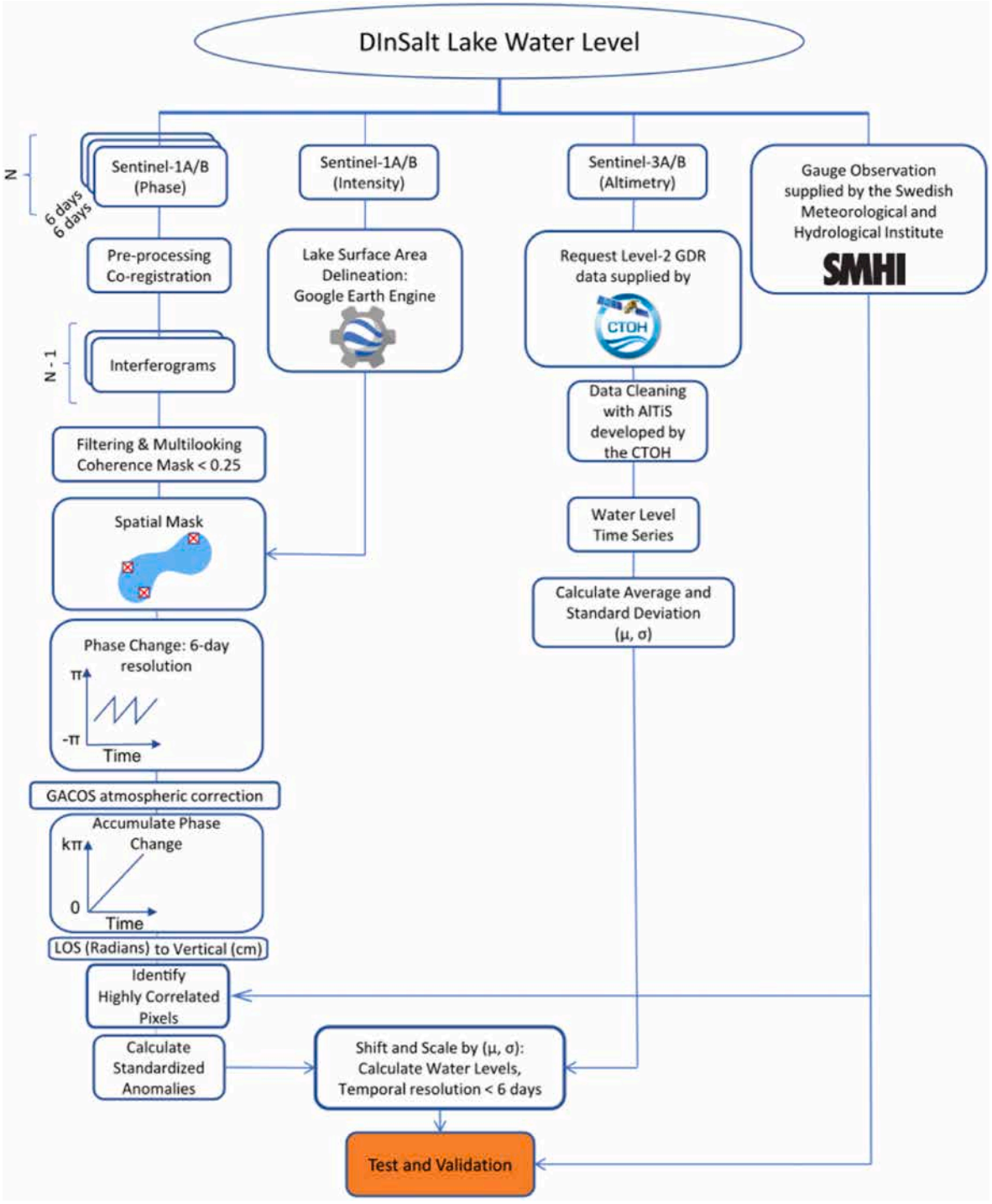

Fig. 2. The procedure of lake water level estimation by combining D-InSAR and altimetry (DInSAlt). First, the six-day water level anomalies are estimated using the D-InSAR method, then scaled and shifted by the satellite altimetry-derived water levels, and finally, the results are tested and validated by the gauged observations.

the anomalies of h_D and h_G (deviation from the average) have similar patterns. Therefore, we can obtain similar magnitudes by scaling the anomalies of h_D and h_G with their standard deviation. As a result, the standardized anomalies of water level from D-InSAR and in-situ observations (SA_D and SA_G) are calculated as:

$$SA_D = (h_D - \mu_D) / \sigma_D \quad (5)$$

$$SA_G = (h_G - \mu_G) / \sigma_G \quad (6)$$

where μ and σ are the average and the standard deviation of gauged and D-InSAR water levels (h_G and h_D).

Standardized anomalies are usually used in meteorology and climatology to predict extreme weather events (Grumm and Hart, 2001). To obtain accurate water levels, we scale and shift the D-InSAR estimation of water level anomalies by the μ and σ of the actual water levels in the same seasons of the D-InSAR data period. However, instead of using the gauged observations, we calculate μ and σ of the satellite altimetry data for the ten lakes and scale and shift the SA_D by these values (Eq. (8)):

$$h_{D,A} = (SA_D \times \sigma_{h_A}) + \mu_{h_A} \quad (7)$$

where $h_{D,A}$ is the final water level derived by DInSAlt, and μ_{hA} and σ_{hA} are the μ and σ of the satellite altimetry-derived water levels (h_A). Hence, this procedure improves the temporal resolution of altimetry-derived water levels by adding data points on a six-day temporal resolution.

For the lakes with more than eight cycles of altimetry data during the same period of the Sentinel-1 SAR acquisitions (late spring to late autumn 2019), we use only the altimetry-derived water levels in 2019 to calculate μ and σ. For the lakes with less than eight cycles of altimetry data in 2019, we use all years of altimetry-derived water levels within the same season (late spring to late autumn from 2016 to 2021).

For validation, we use in-situ water levels provided by the SMHI and calculate Pearson's correlation coefficient (R), Lin's Concordance Correlation Coefficient (CCC), and Root Mean Square Error (RMSE) in the ten lakes. To remove the vertical datum bias, we calculate the difference between the average of the in-situ and DInSAlt water levels and subtract this difference from all of the gauged observations. Therefore, the vertical reference of water levels is the geoid EGM2008.

3. Results

3.1. D-InSAR water level anomalies

For the D-InSAR processing, only interferograms with a six-day separation between SAR pairs were generated during the ice-free period of 2019. Fig. 3 illustrates the sequence of the images (numbers) and the generated interferograms, using the case of Lake Vättern (Fig. 4a), with 29 Sentinel-1A/B images from May 24 to November 8, 2019, leading to 28 interferograms (solid lines) in this period.

The short temporal baseline resulted in high-quality interferograms and smooth fringe patterns in the lake's surroundings (Fig. 4b; phase change in one interferogram between July 11 and July 17, 2019). On the other hand, only a limited number of pixels with high coherence values could be identified ($C > 0.25$) on the lake's surface area, which are located close to the lake's shore, as the trees along the shore are a suitable medium for the SAR double-bounce backscattering (Fig. 4c). Fig. 4d shows the Pearson's correlation (R) between the accumulated phase change across all interferograms (h_D) and the time series of in-situ water level (h_G) for some pixels.

We found that Pearson's correlation between D-InSAR and in-situ water levels (h_D and h_G) in the best pixel of each lake is high ($R > 0.68$), but Lin's correlation is only high when water level changes are small (Fig. 5). The deviation of the best-fit line from the 1:1 line in Fig. 5 shows that h_D values are very different from h_G values (low CCC). However, h_D and h_G have similar variability as the data points in Fig. 5 are closely distributed around the best-fit line (High R). This can be explained by the direction of the water level time series (i.e., increase or decrease), which is well replicated by the D-InSAR method. Yet, the D-InSAR alone cannot predict the exact magnitude of the water level, or at least when the changes in water levels are larger than the wavelength of the SAR signal (Aminjafari et al., 2024b).

The high R-values between D-InSAR and gauged water levels in all lakes (above 0.68; Fig. 5) imply that their standardized anomalies are similar, evident from the time series of such anomalies (Fig. 6). Therefore, Lin's correlations between the standardized anomalies SA_D and SA_G are high. SA_D and SA_G range between −2 and +3 in all lakes and have a decreasing trend between late June and early October as the water level decreases in the summer period.

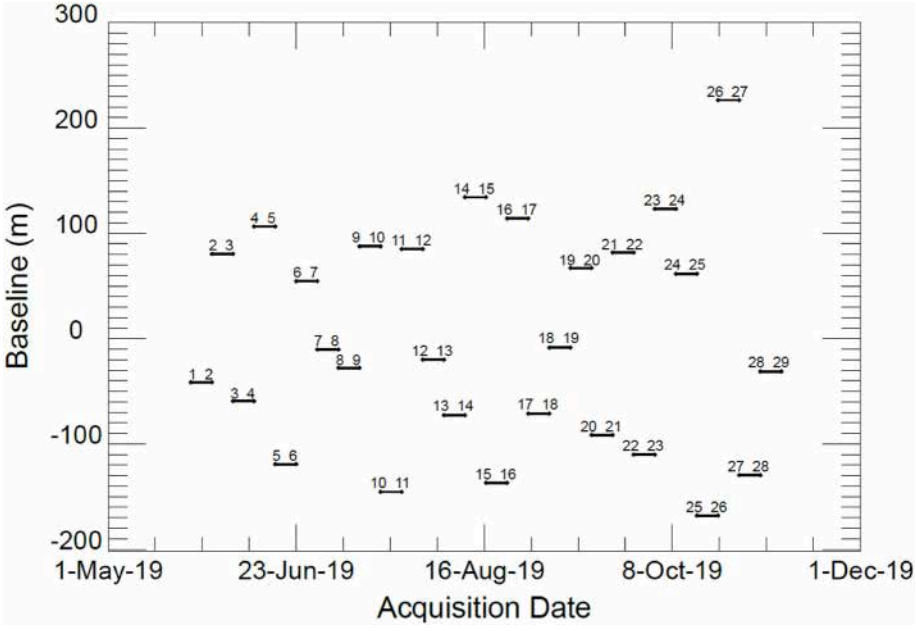

Fig. 3. Baseline and acquisition dates of the six-day 28 interferograms (solid lines) processed for Lake Vättern based on 29 Sentinel-1A/B images (points with numbers). The baseline is the distance between the satellite locations during the two acquisitions.

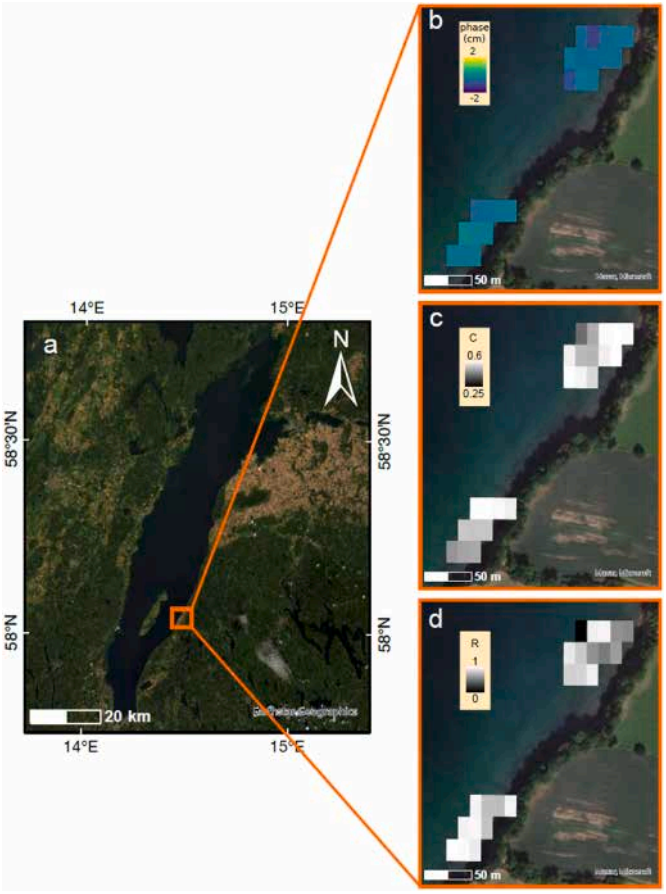

Fig. 4. Lake Vättern: (a) the location of the lake, **(b)** the wrapped vertical phase change between the acquisitions on July 11 and July 17, 2019, after spatial and coherence mask and tropospheric correction **(c)** the coherence map of the corresponding interferogram, **(d)** and Pearson's correlation (R) between the accumulated phase change across all interferograms (h_D) and in-situ water levels (h_G).

3.2. Satellite altimetry water levels

Fig. 7 shows daily in-situ water levels (h_G) and satellite altimetry water levels (h_A) after cleaning the radar altimetry observations. The availability period of the Sentinel-3 altimetry observations is from March 2016 to January 2021 for all lakes except for Lake Mälaren and Lake Båven, as only Sentinel-3B data were available over these two lakes during the nominal orbit phase starting in December 2018. In wide lakes along the satellite track, high-accuracy water levels are generally achieved, and data cleaning is simpler. The best altimetric estimations occur in lakes Möckeln and Vänern (6.6 and 65 km along-track width) with a very high Lin's correlation between h_G and h_A for approximately five years (Fig. 7; CCC = 0.98 and 0.97).

The lowest Lin's correlation between h_G and h_A occurs in Lake Mälaren (CCC = 0.75) as the ground track with extended coverage over this lake (17.5 km, S-3B 483) is far from the gauging station (≈100 km) and may not represent the simultaneous water level of the measuring gauge. Also, many islands on Lake Mälaren affect the satellite observations and result in low CCC between h_G and h_A (Fig. 7). The ground tracks near the gauging station (S-3A track 597, S3B track 272) cover less than 1.5 km of Lake Mälaren, and given the 300 m footprint of the Sentinel-3 altimeter, the standard deviations of the radar altimetry observations do not reach a low value even after several stages of data cleaning.

3.3. DInSAlt (altimetry + D-InSAR) water levels

Once applying DInSAlt, we find that Lin's correlations between gauged- and DInSAlt water level estimates are higher than 0.5 in all lakes, and the best estimations by the DInSAlt method occur in eight lakes with CCC > 0.8 (Fig. 8a) where both altimetry-only water levels (h_A) and D-InSAR water level anomalies (SA_D) have high correlations with in-situ observations (Fig. 8b–c).

The lowest correlations between $h_{D,A}$ and h_G occur in two lakes, Kaalasjärvi and Mälaren, with CCC = 0.65 and CCC = 0.57, respectively (Fig. 8a). This is because Lake Kaalasjärvi has the lowest estimates of water level anomalies by the D-InSAR method among all ten lakes (Fig. 8c), leading to a lower correlation between $h_{D,A}$ and h_G than in the other lakes (Fig. 8a). Underestimation was observed in Lake Kaalasjärvi, where rapid changes in water levels due to snowmelt exceeded the SAR signal's wavelength, leading to lower correlations between DInSAlt and gauged water levels. In Lake Mälaren, the DInSAlt method showed a tendency to overestimate water levels during peak periods, likely due to the limited number of altimetry observations and the influence of land contamination from numerous small islands. Lake Mälaren is an example of poor estimates of altimetry-only water levels (Fig. 8b), resulting in a low correlation between $h_{D,A}$ and h_G (Fig. 8a). We analyzed the root mean square error (RMSE) to quantify these uncertainties and found that lakes with higher quality and higher density of altimetry observations (e.g., Lake Vänern) had lower RMSE values, indicating higher accuracy. In contrast, lakes with more complex shorelines and low-quality altimetry data (e.g., Lake Kaalasjärvi) showed higher RMSE values, reflecting greater uncertainties.

The water level time series in Fig. 9 shows the importance of the DInSAlt method in increasing the density of water level observations by coupling altimetry water levels with D-InSAR water level anomalies. For example, in lakes Torneträsk, Virihaure, and Tjeggelvas, the peaks of water levels between June and August cannot be captured by altimetry-only water levels due to the low density of observations, but with the DInSAlt method, we can spot the time of the peaks and troughs in the water level time series (Fig. 9, arrows on the panels of the right column).

In general, the temporal resolutions of water levels are considerably improved in all lakes with DInSAlt, especially in those lakes where satellite altimetry observations are scarce. Owing to the short revisiting time of the Sentinel-1 constellation (6 days), DInSAlt can achieve temporal resolutions of less than six days. The best improvement occurs in Lake Vänern (2.5 days temporal resolution), where the frequency of the observations doubles that of altimetry-only data (Fig. 10).

4. Discussion

Satellite altimetry observations have been combined with D-InSAR water levels in other studies, but only for the case of wetlands, to derive absolute water level changes from the relative unwrapped interferometric phase (Cao et al., 2018, p. 2; Lu et al., 2009; Yuan et al., 2017; Zhang et al., 2016). In a novel way, we combined these two technologies to improve lake water level detection from space. We find that the DInSAlt method improves the temporal resolution of retrieved water levels from space in large and small lakes. However, its performance depends on the specific conditions of the D-InSAR application and the quality of the satellite altimetry observations. Aminjafari et al. (2024b) showed that marsh-dominated wetlands and forests near a lake are ideal for double-bounce backscattering, resulting in several coherent pixels near the shores of the lakes. In the same way, cliffs or large rocks around the lake may also enable a double-bounce backscattering, as observed in high-altitude lakes in Ecuador (Palomino-Ángel et al., 2022). It is important to consider the potential biases and uncertainties inherent in the method. Our validation process revealed instances of overestimation and underestimation, influenced by several factors including the quality and frequency of altimetry observations, and the presence of coherent scatterers for SAR signal processing. Biases in the DInSAlt method were

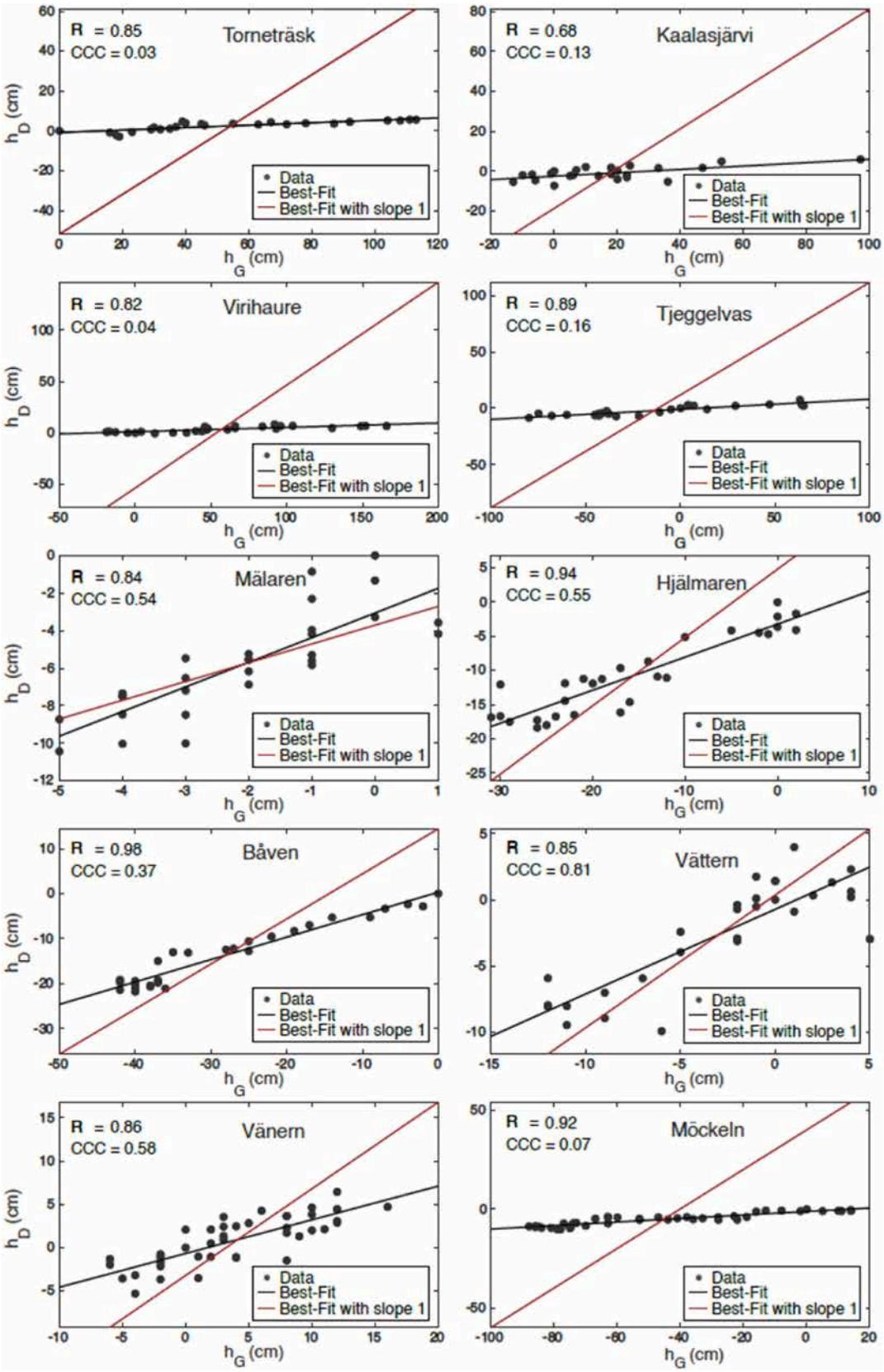

Fig. 5. The scatter plot of in-situ water levels (h_G; cm) vs. D-InSAR water levels (h_D; cm) for ten lakes. The deviation of the best-fit line from the 1:1 line shows that the exact values of water level are not well estimated by D-InSAR (low CCC), but the direction of the change in water level time series is well estimated as the data points are close to the best-fit line (high R).

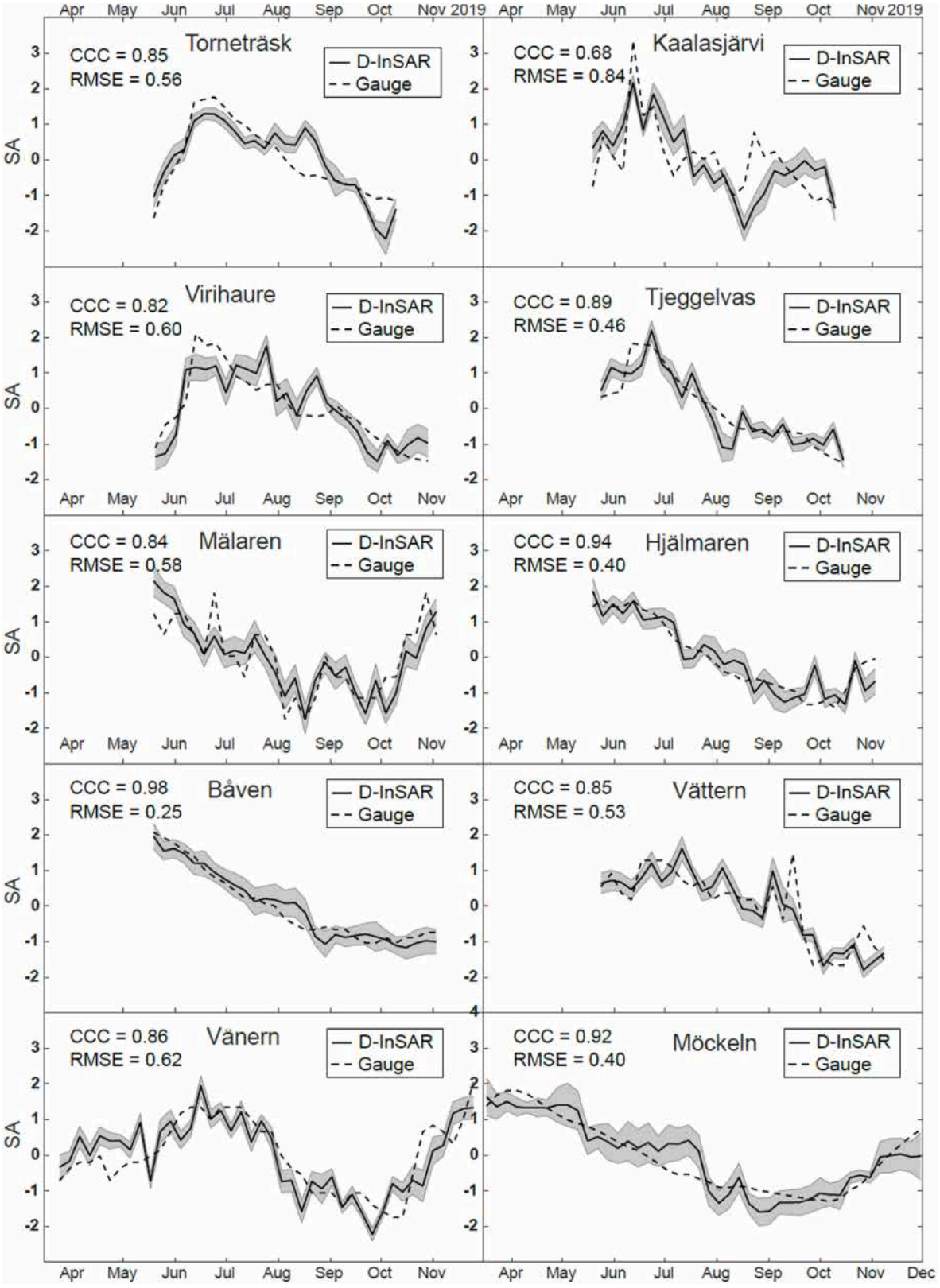

Fig. 6. The time series of the standardized anomalies for the gauged- and D-InSAR water levels in 10 lakes. The observation frequency for both gauged- and D-InSAR is six days. The shaded gray area shows the SA_D uncertainties for the pixels inside the 1×1 km^2 box containing the reference point.

particularly evident in lakes with complex shorelines and significant land contamination, such as Lake Mälaren. Here, the presence of numerous islands and the limited ground track coverage resulted in overestimation during peak water levels. Similarly, in high-altitude lakes like Lake Kaalasjärvi, rapid water level changes due to snowmelt led to underestimation, as the SAR signal's wavelength was insufficient to capture these rapid fluctuations. Therefore, some level of bias remains, which should be considered when interpreting the results.

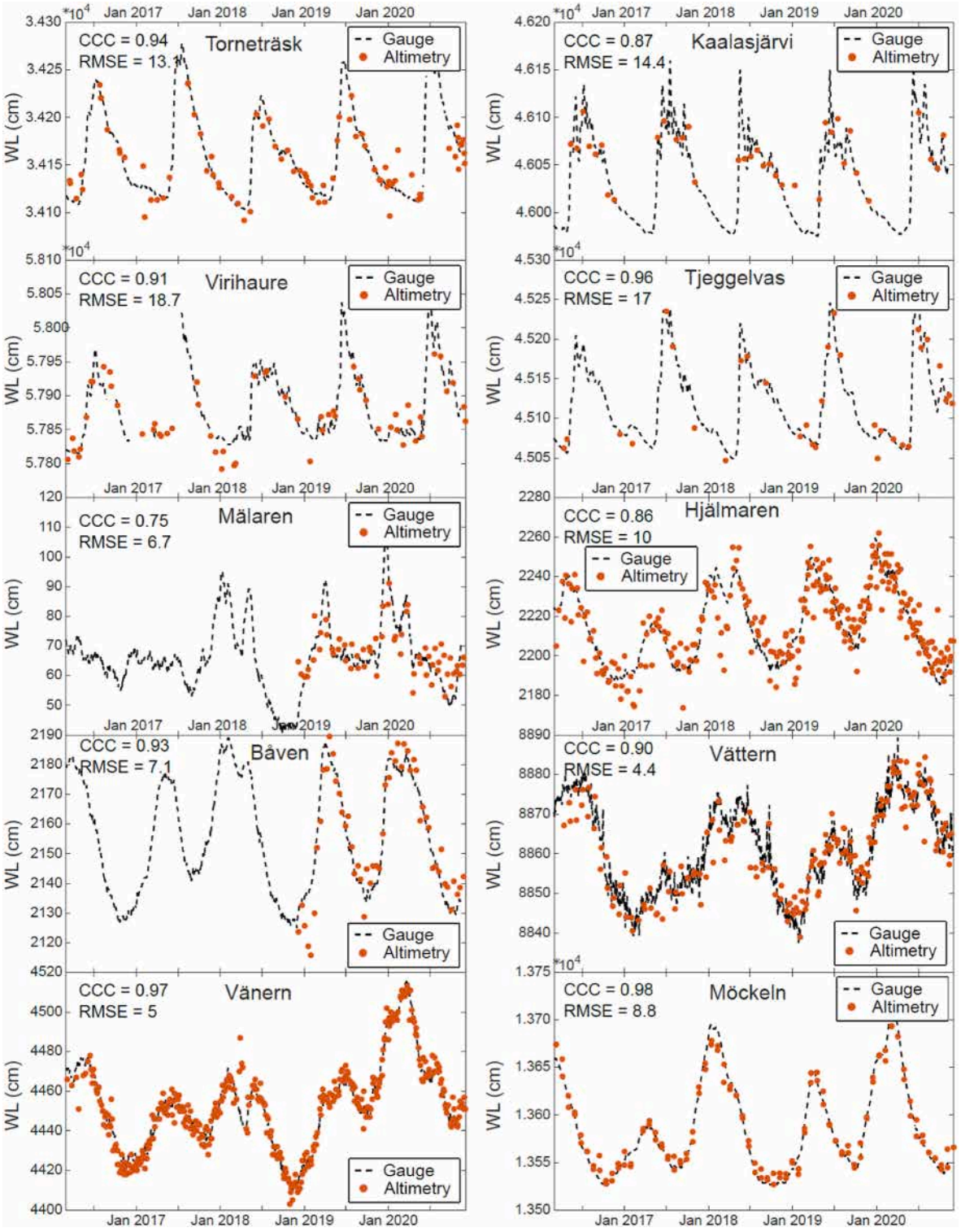

Fig. 7. The time series of water level (WL) from altimetry-only observations of Sentinel-3 and gauge observations between Mar 2016 and Jan 2021. The dashed line represents gauge observations and the orange circles are altimetry water levels. (For interpretation of the references to colour in this figure legend, the reader is referred to the Web version of this article.)

The number and the length of the satellite ground tracks crossing over the lake's surface area also play an important role in the performance of this method. For example, in Lake Mälaren, with low CCC between DInSAlt- and in-situ water levels (CCC = 0.18) compared to other lakes, only a short portion of the satellite ground tracks (<1.5 km) are crossing over the lake surface area near the gauging station. Even for the ground tracks farther from the station, the land contamination, due to the high number of small islands all over the lake, deteriorates the quality of the radar altimetry measurements and leads to inaccurate water levels.

It is worth noting that a low number of altimetry observations can still result in high correlations between DInSAlt- and gauged water levels, such as the cases of lakes Virihaure and Tjeggelvas, where a few altimetry-derived observations (5 and 3, respectively) result in high

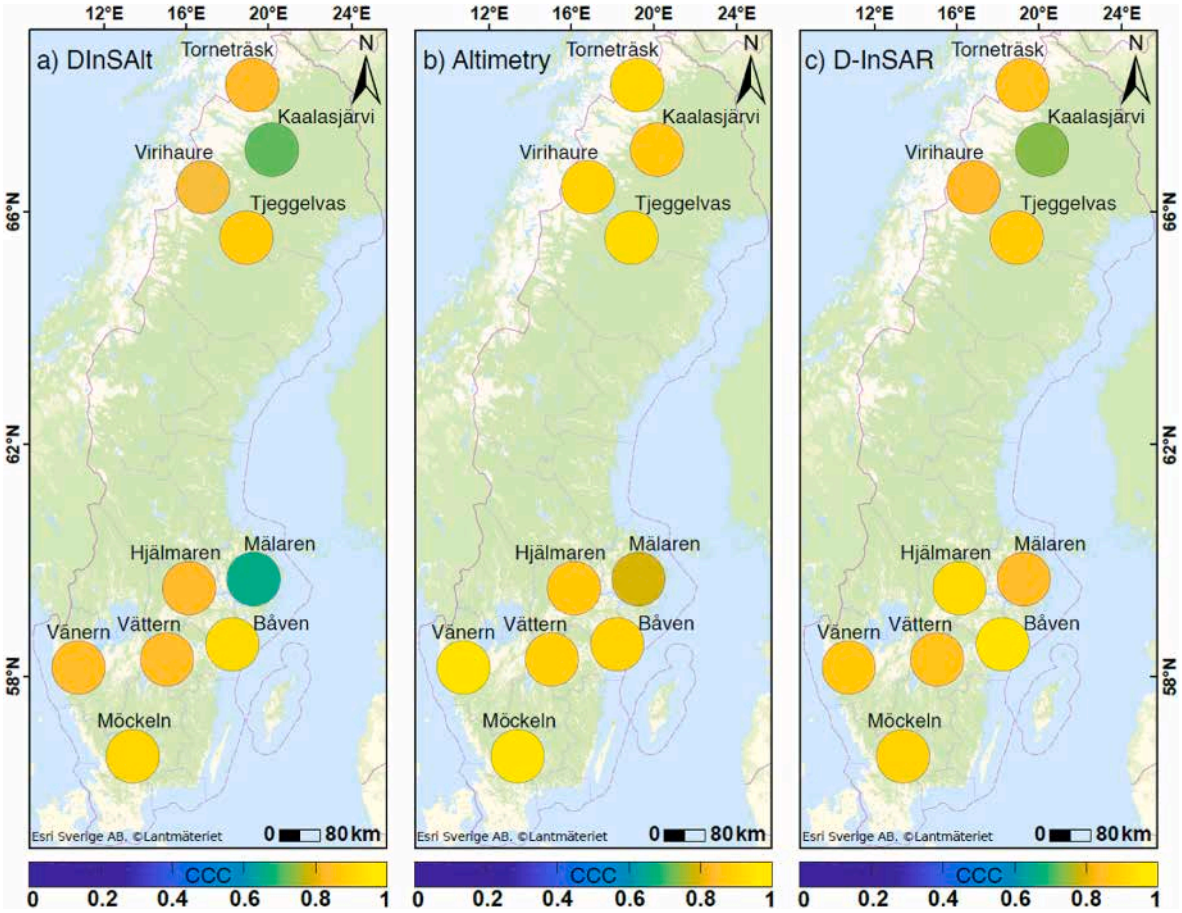

Fig. 8. **(a)** Lin's correlation (CCC) between in-situ and estimated DInSAlt water levels and, **(b)** between in-situ and altimetry-only water levels and, **(c)** between in-situ and D-InSAR water level anomalies. For altimetry-only water levels, the correlation was calculated based on five-year data, and for DInSAlt water levels, based on one-year data (2019).

correlations after applying DInSAlt (0.83 and 0.82, respectively). This is due to long ground tracks (6.1 km and 4.5 km, respectively) over the lakes' surface areas, which produce accurate measurements of the range between the satellite and the water surface (low land-contaminated signal). Therefore, as long as one satellite altimetry ground track covers a sufficient area of the lake's surface, the DInSAlt estimations are consistent with the actual water levels.

As the lakes in this study are distributed across the Swedish landscape and latitudinal gradient, DInSAlt's performance is subject to the specific characteristics of the lakes. However, when water level changes often exceed the full cycle of the phase change of the SAR signal between acquisitions in lakes with smaller surface areas and higher altitudes, anomalies of the actual water levels are not precise (Aminjafari et al., 2024b). As a result, the DInSAlt does not perform well in lakes with frequent large changes in water levels.

It is worth highlighting for potential users of DInSAlt that the presence of more than one scatterer in one SAR cell increases the risk of the Radar speckle that can affect some of the coherent pixels in SAR images (Aminjafari et al., 2024b; Karimi and Taban, 2021). Hence, careful attention is needed when choosing interferometric pixels to estimate water level anomalies. Applying conventional filtering (e.g., muti-looking and Goldenstein filter) can reduce noise (Aminjafari et al., 2024b), and using the median of the coherent pixels can moderate the risk of reliance on a few pixels.

In our study, identifying D-InSAR pixels that exhibit standardized anomalies correlating with in-situ water levels relied on in-situ measurements. This approach inherently limits the scalability and applicability of our findings, especially in regions where such measurements are unavailable. However, the recently launched Surface Water and Ocean Topography (SWOT) satellite significantly expands the potential use of our framework. SWOT was jointly developed by NASA and the French Space Agency (CNES: Center national d'études spatiales) in partnership with the Canadian Space Agency (CSA) and the United Kingdom Space Agency (UKSA). SWOT's small-incidence angle InSAR technology is designed to provide precise and comprehensive water surface measurements across vast geographic scales with ~4 observations per 21 days in high latitudes (Aminjafari et al., 2024a). This capability allows for identifying relevant D-InSAR pixels without the direct dependence on in-situ data and enhances our ability to monitor and analyze water levels in remote or ungauged water bodies. Therefore, SWOT can potentially expand the geographical applicability of our findings and reduce the reliance on ground measurements.

The DInSAlt method could be further improved by using future technologies. For example, its use on upcoming SAR missions with long-wavelength images (L-Band and S-Band), such as the NASA-ISRO SAR (NISAR) mission to be launched in 2025 (Rosen and Kumar, 2021) that can measure water levels below dense canopy with tall vegetation covers.

5. Conclusion

In this study, we use D-InSAR to improve the temporal resolution of altimetry water level measurements using a new methodology called DInSAlt. We test and validate the methodology across ten lakes in Sweden with on-site gauged observations. We found that DInSAlt successfully estimated the actual water levels in eight of ten lakes in Sweden

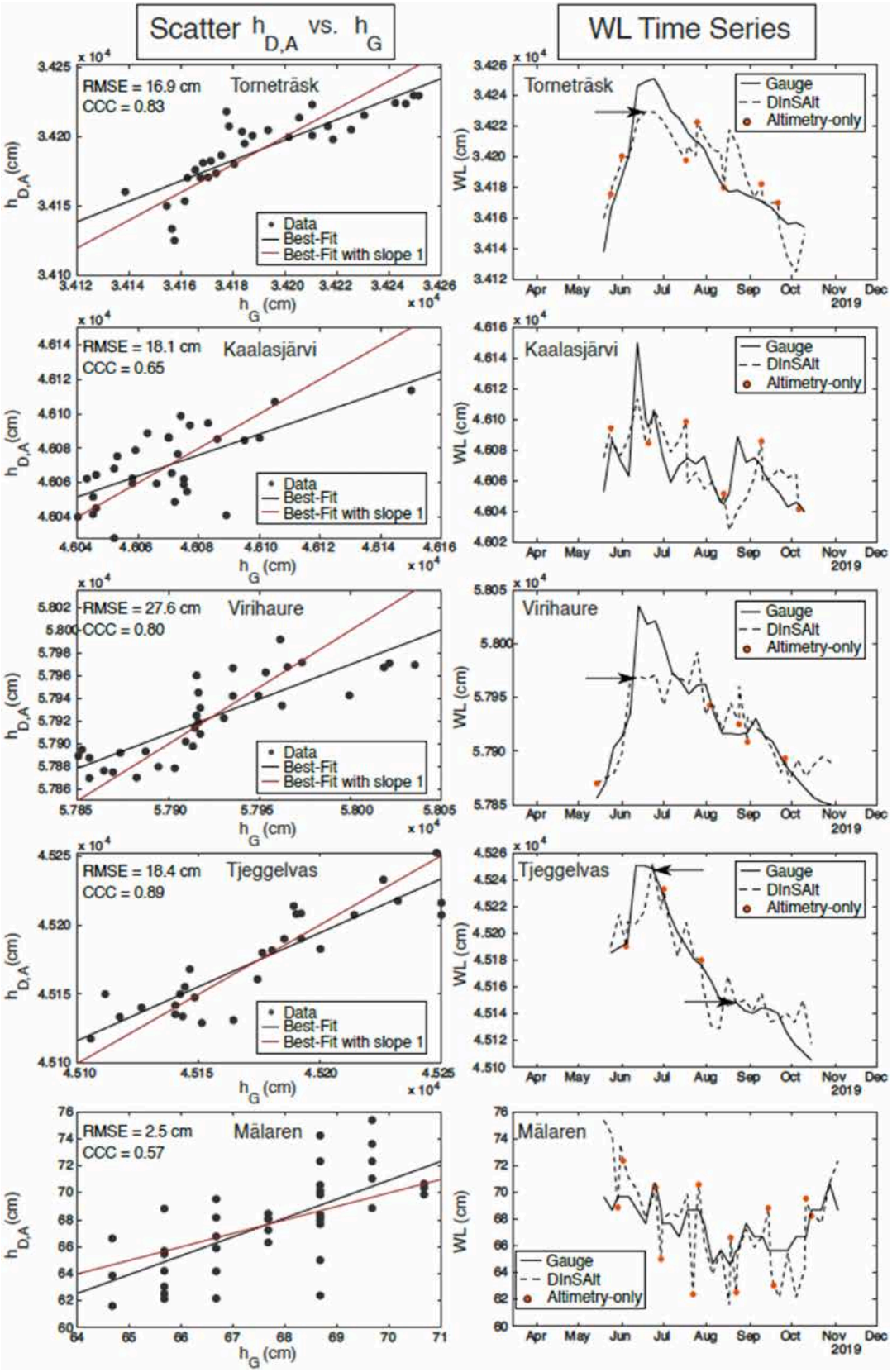

Fig. 9. The comparison between in-situ water levels (h_G) and DInSAlt water levels ($h_{D,A}$) for 10 lakes. **Left column:** the scatter plot of h_G vs $h_{D,A}$. **Right column:** water level time series (WL) in 2019. The orange points show satellite altimetry observations. Arrows show some examples of the peaks and troughs not captured by altimetry-only observations but by the DInSAlt. Continues to the next page. (For interpretation of the references to colour in this figure legend, the reader is referred to the Web version of this article.)

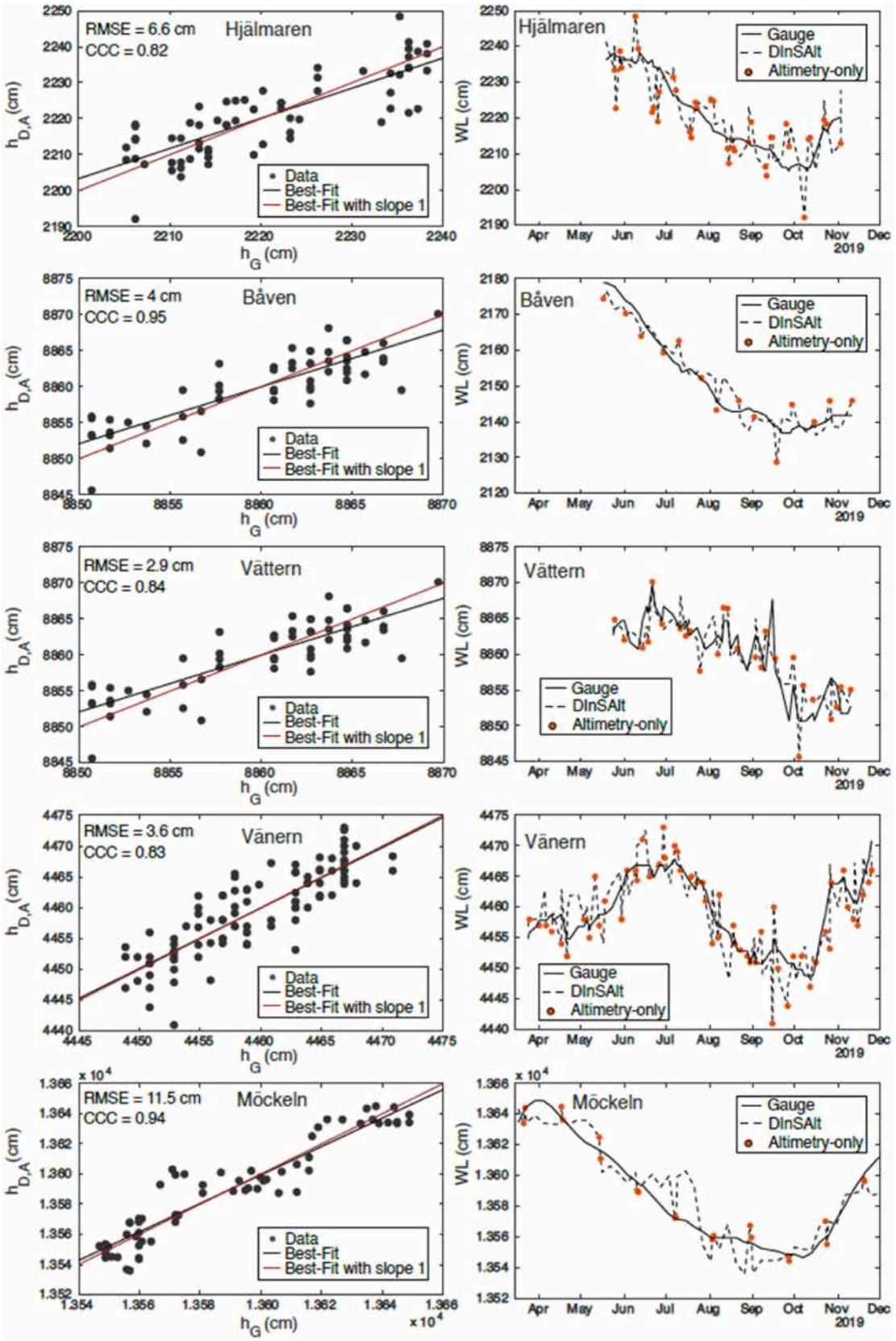

Fig. 9. (*continued*).

and increased the temporal resolution of altimetry water level measurements. The accuracy of water level estimation was highest in lakes with long ground satellite altimetry passing over the lake surface and with suitable conditions for a double-bounce backscattering of the SAR signal. The DInSAlt methodology can be applied to both large and small lakes in both mountainous and flat areas and can capture both subtle and

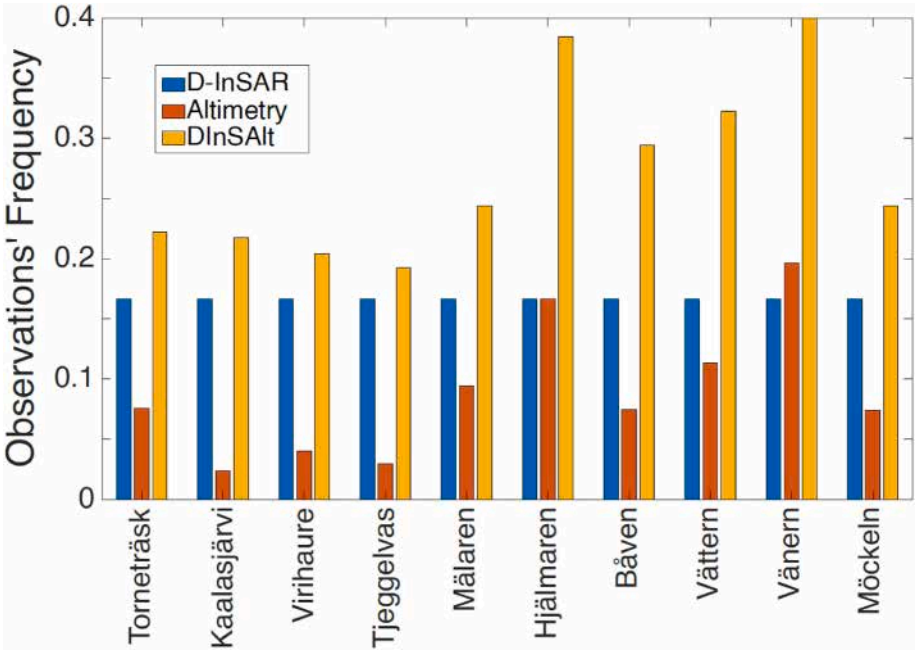

Fig. 10. Frequency of observations available from D-InSAR water level anomalies (SA_D), altimetry-only water levels (h_A), and DInSAlt water levels ($h_{D,A}$).

rapid changes in water levels that cannot be obtained with D-InSAR or altimetry data alone. The inclusion of multi-sensor altimetry data remains a valuable future direction. Future studies with longer observation periods and enhanced altimetry datasets may further explore the integration of these multi-sensor approaches for comprehensive lake monitoring. The DInSAlt methodology can benefit from the data of the newly launched SWOT satellite for lake water level estimation without relying on in-situ measurements.

CRediT authorship contribution statement

Saeid Aminjafari: Writing – review & editing, Writing – original draft, Visualization, Validation, Software, Project administration, Methodology, Investigation, Formal analysis, Data curation, Conceptualization. **Frédéric Frappart:** Writing – review & editing, Software, Methodology, Data curation, Conceptualization. **Fabrice Papa:** Writing – review & editing, Software, Methodology, Data curation, Conceptualization. **Ian Brown:** Writing – review & editing, Supervision, Software, Methodology, Data curation, Conceptualization. **Fernando Jaramillo:** Writing – review & editing, Writing – original draft, Supervision, Resources, Project administration, Methodology, Investigation, Funding acquisition, Data curation, Conceptualization.

Declaration of competing interest

The authors declare that they have no known competing financial interests or personal relationships that could have appeared to influence the work reported in this paper.

Data availability

Data will be made available on request.

Acknowledgments

This work was funded by the Swedish National Space Agency (180/18), the Swedish Research Council (VR) Project 2021–05774, and the Baltic Sea Centre, Stockholm University.

Appendix A. Supplementary data

Supplementary data to this article can be found online at https://doi.org/10.1016/j.srs.2024.100162.

References

Abdalla, S., et al., 2021. Altimetry for the future: building on 25 years of progress. Advances in Space Research, 25 Years of Progress in Radar Altimetry 68, 319–363. https://doi.org/10.1016/j.asr.2021.01.022.

Abileah, R., Vignudelli, S., 2021. Precise inland surface altimetry (PISA) with nadir specular echoes from Sentinel-3: algorithm and performance assessment. Rem. Sens. Environ. 264, 112580 https://doi.org/10.1016/j.rse.2021.112580.

Abrams, M., Crippen, R., Fujisada, H., 2020. ASTER global digital elevation model (GDEM) and ASTER global water body dataset (ASTWBD). Rem. Sens. 12, 1156. https://doi.org/10.3390/rs12071156.

Alsdorf, D.E., Melack, J.M., Dunne, T., Mertes, L.A.K., Hess, L.L., Smith, L.C., 2000. Interferometric radar measurements of water level changes on the Amazon flood plain. Nature 404, 174–177. https://doi.org/10.1038/35004560.

Alsdorf, D.E., Rodríguez, E., Lettenmaier, D.P., 2007. Measuring surface water from space. Rev. Geophys. 45 https://doi.org/10.1029/2006RG000197.

Aminjafari, S., Brown, I.A., Frappart, F., Papa, F., Blarel, F., Mayamey, F.V., Jaramillo, F., 2024a. Distinctive patterns of water level change in Swedish lakes driven by climate and human regulation. Water Resour. Res. 60, e2023WR036160 https://doi.org/10.1029/2023WR036160.

Aminjafari, S., Brown, I., Mayamey, F.V., Jaramillo, F., 2024b. Tracking centimeter-scale water level changes in Swedish lakes using D-InSAR. Water Resour. Res. 60, e2022WR034290 https://doi.org/10.1029/2022WR034290.

Bamber, J.L., 1994. Ice sheet altimeter processing scheme. Int. J. Rem. Sens. 15, 925–938. https://doi.org/10.1080/01431169408954125.

Bandini, F., Jakobsen, J., Olesen, D., Reyna-Gutierrez, J.A., Bauer-Gottwein, P., 2017. Measuring water level in rivers and lakes from lightweight Unmanned Aerial Vehicles. J. Hydrol. 548, 237–250.

Barzegar, R., Aalami, M.T., Adamowski, J., 2021. Coupling a hybrid CNN-lstm deep learning model with a boundary corrected maximal overlap discrete wavelet transform for multiscale lake water level forecasting. J. Hydrol. 598, 126196 https://doi.org/10.1016/j.jhydrol.2021.126196.

Baup, F., Frappart, F., Maubant, J., 2014. Combining high-resolution satellite images and altimetry to estimate the volume of small lakes. Hydrol. Earth Syst. Sci. 18, 2007–2020. https://doi.org/10.5194/hess-18-2007-2014.

Biancamaria, S., Frappart, F., Leleu, A.-S., Marieu, V., Blumstein, D., Desjonquères, J.-D., Boy, F., Sottolichio, A., Valle-Levinson, A., 2017. Satellite radar altimetry water elevations performance over a 200m wide river: evaluation over the Garonne River. Adv. Space Res. 59, 128–146. https://doi.org/10.1016/j.asr.2016.10.008.

Biancamaria, S., Schaedele, T., Blumstein, D., Frappart, F., Boy, F., Desjonquères, J.-D., Pottier, C., Blarel, F., Niño, F., 2018. Validation of Jason-3 tracking modes over French rivers. Rem. Sens. Environ. 209, 77–89. https://doi.org/10.1016/j.rse.2018.02.037.

Boy, F., Poisson, J.C., Fouqueau, V., Picot, N., Le Gac, S., 2023. Measuring longitudinal river profiles from Sentinel-6 Fully-Focused SAR mode. In: 2023 Ocean Surface Topography Science Team Meeting, p. 96. https://doi.org/10.24400/527896/a03-2023.3781.

Cao, N., Lee, H., Jung, H.C., Yu, H., 2018. Estimation of water level changes of large-scale amazon wetlands using ALOS2 ScanSAR differential interferometry. Rem. Sens. 10, 966. https://doi.org/10.3390/rs10060966.

Chen, Z., White, L., Banks, S., Behnamian, A., Montpetit, B., Pasher, J., Duffe, J., Bernard, D., 2020. Characterizing marsh wetlands in the great lakes basin with C-band InSAR observations. Rem. Sens. Environ. 242, 111750 https://doi.org/10.1016/j.rse.2020.111750.

Cooley, S.W., Ryan, J.C., Smith, L.C., 2021. Human alteration of global surface water storage variability. Nature 591, 78–81. https://doi.org/10.1038/s41586-021-03262-3.

Cretaux, J.-F., Nielsen, K., Frappart, F., Papa, F., Calmant, S., Benveniste, J., 2017. Hydrological applications of satellite AltimetryRivers, lakes, man-made reservoirs, inundated areas. In: Satellite Altimetry over Oceans and Land Surfaces. CRC Press.

Farr, T.G., Kobrick, M., 2000. Shuttle radar topography mission produces a wealth of data. Eos, Transactions American Geophysical Union 81, 583–585. https://doi.org/10.1029/EO081i048p00583.

Frappart, F., Blarel, F., Fayad, I., Bergé-Nguyen, M., Crétaux, J.-F., Shu, S., Schregenberger, J., Baghdadi, N., 2021. Evaluation of the performances of radar and lidar altimetry missions for water level retrievals in mountainous environment: the case of the Swiss lakes. Rem. Sens. 13, 2196. https://doi.org/10.3390/rs13112196.

Frappart, F., Calmant, S., Cauhopé, M., Seyler, F., Cazenave, A., 2006. Preliminary results of ENVISAT RA-2-derived water levels validation over the Amazon basin. Rem. Sens. Environ. 100, 252–264. https://doi.org/10.1016/j.rse.2005.10.027.

Goldstein, R.M., Werner, C.L., 1998. Radar interferogram filtering for geophysical applications. Geophys. Res. Lett. 25, 4035–4038. https://doi.org/10.1029/1998GL900033.

Grumm, R.H., Hart, R., 2001. Standardized anomalies applied to significant cold season weather events: preliminary findings. Weather Forecast. 16, 736–754. https://doi.org/10.1175/1520-0434(2001)016<0736:SAATSC>2.0.CO;2.

Hong, S.H., Wdowinski, S., Kim, S.W., 2010. Evaluation of TerraSAR-X observations for wetland InSAR application. IEEE Trans. Geosci. Rem. Sens. 48, 864–873. https://doi.org/10.1109/TGRS.2009.2026895.

Jaramillo, F., Brown, I., Castellazzi, P., Espinosa, L., Guittard, A., Hong, S.-H., Rivera-Monroy, V.H., Wdowinski, S., 2018. Assessment of hydrologic connectivity in an ungauged wetland with InSAR observations. Environ. Res. Lett. 13, 024003 https://doi.org/10.1088/1748-9326/aa9d23.

Kao, Y.-C., Rogers, M.W., Bunnell, D.B., Cowx, I.G., Qian, S.S., Anneville, O., Beard, T.D., Brinker, A., Britton, J.R., Chura-Cruz, R., Gownaris, N.J., Jackson, J.R., Kangur, K., Kolding, J., Lukin, A.A., Lynch, A.J., Mercado-Silva, N., Moncayo-Estrada, R., Njaya, F.J., Ostrovsky, I., Rudstam, L.G., Sandström, A.L.E., Sato, Y., Siguayro-Mamani, H., Thorpe, A., van Zwieten, P.A.M., Volta, P., Wang, Y., Weiperth, A., Weyl, O.L.F., Young, J.D., 2020. Effects of climate and land-use changes on fish catches across lakes at a global scale. Nat. Commun. 11, 2526. https://doi.org/10.1038/s41467-020-14624-2.

Karimi, N., Taban, M.R., 2021. A convex variational method for super resolution of SAR image with speckle noise. Signal Process. Image Commun. 90, 116061 https://doi.org/10.1016/j.image.2020.116061.

Larson, M., 2012. Sweden's great lakes. In: Bengtsson, L., Herschy, R.W., Fairbridge, R. W. (Eds.), Encyclopedia of Lakes and Reservoirs. Springer, Netherlands, Dordrecht, pp. 761–764. https://doi.org/10.1007/978-1-4020-4410-6_269.

Liu, D., Wang, X., Aminjafari, S., Yang, W., Cui, B., Yan, S., Zhang, Y., Zhu, J., Jaramillo, F., 2020. Using InSAR to identify hydrological connectivity and barriers in a highly fragmented wetland. Hydrol. Process. 34, 4417–4430. https://doi.org/10.1002/hyp.13899.

Lu, Z., Kim, J.-W., Lee, H., Shum, C.K., Duan, J., Ibaraki, M., Akyilmaz, O., Read, C.-H., 2009. Helmand River hydrologic studies using ALOS PALSAR InSAR and ENVISAT altimetry. Mar. Geodesy 32, 320–333. https://doi.org/10.1080/01490410903094833.

Magsar, A., Matsumoto, T., Enkhbold, A., Nyam-Osor, N., 2021. Application of remote sensing and gis techniques for the analysis of Lake water fluctuations: a case study of ugii lake. Mongolia. NEPT 20. https://doi.org/10.46488/NEPT.2021.v20i05.022.

Markus, T., Neumann, T., Martino, A., Abdalati, W., Brunt, K., Csatho, B., Farrell, S., Fricker, H., Gardner, A., Harding, D., Jasinski, M., 2017. The Ice, Cloud, and land Elevation Satellite-2 (ICESat-2): science requirements, concept, and implementation. Rem. Sens. Environ. 190, 260–273. https://doi.org/10.1016/j.rse.2016.12.029.

Myrzakhmetov, A., Dostay, Z., Alimkulov, S., Tursunova, A., Sarsenova, I., 2022. Level regime of Balkhash Lake as the indicator of the state of the environmental ecosystems of the region. Paddy Water Environ. https://doi.org/10.1007/s10333-022-00890-x.

Palomino-Ángel, S., Vázquez, R.F., Hampel, H., Anaya, J.A., Mosquera, P.V., Lyon, S.W., Jaramillo, F., 2022. Retrieval of simultaneous water-level changes in small lakes with InSAR. Geophys. Res. Lett. 49, e2021GL095950 https://doi.org/10.1029/2021GL095950.

Rosen, P.A., Kumar, R., 2021. NASA-ISRO SAR (NISAR) Mission Status. In: IEEE Radar Conference (RadarConf21), Atlanta, GA, USA, pp. 1–6. https://doi.org/10.1109/RadarConf2147009.2021.9455211.

Ridolfi, E., Manciola, P., 2018. Water level measurements from drones: a pilot case study at a dam site. Water 10, 297.

Shiklomanov, A.I., Lammers, R.B., Vörösmarty, C.J., 2002. Widespread decline in hydrological monitoring threatens Pan-Arctic Research. Eos, Transactions American Geophysical Union 83, 13–17. https://doi.org/10.1029/2002EO000007.

Siles, G., Trudel, M., Peters, D.L., Leconte, R., 2020. Hydrological monitoring of high-latitude shallow water bodies from high-resolution space-borne D-InSAR. Rem. Sens. Environ. 236, 111444 https://doi.org/10.1016/j.rse.2019.111444.

Taburet, N., Zawadzki, L., Vayre, M., Blumstein, D., Le Gac, S., Boy, F., Raynal, M., Labroue, S., Crétaux, J.-F., Femenias, P., 2020. S3MPC: improvement on inland water tracking and water level monitoring from the OLTC onboard sentinel-3 altimeters. Rem. Sens. 12, 3055. https://doi.org/10.3390/rs12183055.

Verron, J., Bonnefond, P., Andersen, O., Ardhuin, F., Bergé-Nguyen, M., Bhowmick, S., Blumstein, D., Boy, F., Brodeau, L., Crétaux, J.-F., Dabat, M.L., Dibarboure, G., Fleury, S., Garnier, F., Gourdeau, L., Marks, K., Queruel, N., Sandwell, D., Smith, W. H.F., Zaron, E.D., 2021. The SARAL/AltiKa mission: a step forward to the future of altimetry. Advances in Space Research, 25 Years of Progress in Radar Altimetry 68, 808–828. https://doi.org/10.1016/j.asr.2020.01.030.

Wdowinski, S., Kim, S.-W., Amelung, F., Dixon, T.H., Miralles-Wilhelm, F., Sonenshein, R., 2008. Space-based detection of wetlands' surface water level changes from L-band SAR interferometry. Rem. Sens. Environ. 112, 681–696. https://doi.org/10.1016/j.rse.2007.06.008.

Wingham, D.J., Rapley, C.G., Griffiths, H., 1986. New techniques in satellite altimeter tracking systems. (No. N8718164). Mullard Space Science Lab., Dorking (England). National Aeronautics and Space Administration, Washington, DC.

Woolway, R.I., Kraemer, B.M., Lenters, J.D., Merchant, C.J., O'Reilly, C.M., Sharma, S., 2020. Global lake responses to climate change. Nat. Rev. Earth Environ. 1 (8), 388–403. https://doi.org/10.1038/s43017-020-0067-5.

Yao, X., Cao, Y., Zheng, G., Devlin, A.T., Li, X., Li, M., Tang, S., Xu, L., 2021. Ecological adaptability and population growth tolerance characteristics of Carex cinerascens in response to water level changes in Poyang Lake, China. Sci. Rep. 11, 4887. https://doi.org/10.1038/s41598-021-84282-x.

Yu, C., Li, Z., Penna, N.T., 2018a. Interferometric synthetic aperture radar atmospheric correction using a GPS-based iterative tropospheric decomposition model. Rem. Sens. Environ. 204, 109–121. https://doi.org/10.1016/j.rse.2017.10.038.

Yu, C., Li, Z., Penna, N.T., Crippa, P., 2018b. Generic atmospheric correction model for interferometric synthetic aperture radar observations. J. Geophys. Res. Solid Earth 123, 9202–9222. https://doi.org/10.1029/2017JB015305.

Yuan, T., Lee, H., Jung, H.C., Aierken, A., Beighley, E., Alsdorf, D.E., Tshimanga, R.M., Kim, D., 2017. Absolute water storages in the Congo River floodplains from integration of InSAR and satellite radar altimetry. Rem. Sens. Environ. 201, 57–72. https://doi.org/10.1016/j.rse.2017.09.003.

Zhang, G., Xie, H., Kang, S., Yi, D., Ackley, S.F., 2011. Monitoring lake level changes on the Tibetan Plateau using ICESat altimetry data (2003–2009). Rem. Sens. Environ. 115 (7), 1733–1742. https://doi.org/10.1016/j.rse.2011.03.005.

Zhang, G., Yao, T., Xie, H., Yang, K., Zhu, L., Shum, C.K., Bolch, T., Yi, S., Allen, S., Jiang, L., Chen, W., 2020. Response of Tibetan Plateau lakes to climate change: trends, patterns, and mechanisms. Earth Sci. Rev. 208, 103269 https://doi.org/10.1016/j.earscirev.2020.103269.

Zhang, M., Li, Z., Tian, B., Zhou, J., Tang, P., 2016. The backscattering characteristics of wetland vegetation and water-level changes detection using multi-mode SAR: a case study. Int. J. Appl. Earth Obs. Geoinf. 45, 1–13. https://doi.org/10.1016/j.jag.2015.10.001.